

# Zoledronic Acid Restores Doxorubicin Chemosensitivity and Immunogenic Cell Death in Multidrug-Resistant Human Cancer Cells

Chiara Riganti<sup>1,2\*</sup>, Barbara Castella<sup>2</sup>, Joanna Kopecka<sup>1</sup>, Ivana Campia<sup>1</sup>, Marta Coscia<sup>2,3</sup>, Gianpiero Pescarmona<sup>1,2</sup>, Amalia Bosia<sup>1,2</sup>, Dario Ghigo<sup>1,2</sup>, Massimo Massaia<sup>2,3</sup>

**1** Department of Oncology, University of Torino, Torino, Italy, **2** Center for Experimental Research and Medical Studies (CeRMS), University of Torino, Torino, Italy, **3** Division of Hematology, University of Torino, Torino, Italy

## Abstract

Durable tumor cell eradication by chemotherapy is challenged by the development of multidrug-resistance (MDR) and the failure to induce immunogenic cell death. The aim of this work was to investigate whether MDR and immunogenic cell death share a common biochemical pathway eventually amenable to therapeutic intervention. We found that mevalonate pathway activity, Ras and RhoA protein isoprenylation, Ras- and RhoA-downstream signalling pathway activities, Hypoxia Inducible Factor-1alpha activation were significantly higher in MDR+ compared with MDR- human cancer cells, leading to increased P-glycoprotein expression, and protection from doxorubicin-induced cytotoxicity and immunogenic cell death. Zoledronic acid, a potent aminobisphosphonate targeting the mevalonate pathway, interrupted Ras- and RhoA-dependent downstream signalling pathways, abrogated the Hypoxia Inducible Factor-1alpha-driven P-glycoprotein expression, and restored doxorubicin-induced cytotoxicity and immunogenic cell death in MDR+ cells. Immunogenic cell death recovery was documented by the ability of dendritic cells to phagocytose MDR+ cells treated with zoledronic acid plus doxorubicin, and to recruit anti-tumor cytotoxic CD8+ T lymphocytes. These data indicate that MDR+ cells have an hyper-active mevalonate pathway which is targetable with zoledronic acid to antagonize their ability to withstand chemotherapy-induced cytotoxicity and escape immunogenic cell death.

**Citation:** Riganti C, Castella B, Kopecka J, Campia I, Coscia M, et al. (2013) Zoledronic Acid Restores Doxorubicin Chemosensitivity and Immunogenic Cell Death in Multidrug-Resistant Human Cancer Cells. PLoS ONE 8(4): e60975. doi:10.1371/journal.pone.0060975

**Editor:** Derya Unutmaz, New York University, United States of America

**Received:** January 24, 2013; **Accepted:** March 1, 2013; **Published:** April 12, 2013

**Copyright:** © 2013 Riganti et al. This is an open-access article distributed under the terms of the Creative Commons Attribution License, which permits unrestricted use, distribution, and reproduction in any medium, provided the original author and source are credited.

**Funding:** Italian Association for Cancer Research (AIRC, www.airc.it; MFAG 11475 to Chiara Riganti, IG 13119 to Massimo Massaia); Italian Ministry of University and Research (www.miur.it; PRIN 2010–2011 to Massimo Massaia, FIRB 2012 to Chiara Riganti); Fondazione Internazionale Ricerche Medicina Sperimentale (www.cerms.it, to Amalia Bosia, Massimo Massaia); Regione Piemonte (Ricerca Sanitaria Finalizzata 2009 to Chiara Riganti, Amalia Bosia; Progetto Immonc to Massimo Massaia). Joanna Kopecka is the recipient of a "Mario and Valeria Rindi" fellowship from Italian Foundation for Cancer Research (FIRC). The funders had no role in study design, data collection and analysis, decision to publish, or preparation of the manuscript.

**Competing Interests:** The authors have declared that no competing interests exist.

\* E-mail: chiara.riganti@unito.it

## Introduction

The mevalonate (Mev) pathway is a highly conserved metabolic cascade which produces sterols, such as cholesterol, and isoprenoids, such as farnesyl pyrophosphate (FPP) and geranylgeranyl pyrophosphate (GGPP). The latter are necessary for the isoprenylation and activity of small G-proteins such as Ras and Rho which control cell proliferation, cytoskeleton remodelling and angiogenesis [1].

Over-expression of Mev pathway enzymes has been correlated with a poor clinical outcome in several human cancers [2,3]. Intracellular cholesterol levels may modulate resistance to a variety of anticancer drugs, within a functional phenotype termed multidrug-resistance (MDR), which can be constitutive or induced after exposure to repeated courses of non-eradicating chemotherapy [4]. The plasma membranes of MDR+ tumor cells are particularly rich in cholesterol which facilitates the activity of P-glycoprotein (Pgp) [5], an integral membrane transporter extruding chemotherapy drugs such as anthracyclines, taxanes, Vinca alkaloids, epipodophyllotoxins, topotecan, and mitomycin C [4]. Another hallmark of MDR+ tumor cells is the increased

isoprenylation and activity of G-proteins which are also dependent on the rate of the Mev pathway activity [6,7].

Accumulating evidence indicates that successful and durable tumor cell eradication is dependent on the ability of chemotherapy drugs to kill tumor cells in a way which is detectable by the immune system. The term immunogenic cell death (ICD) has been coined to describe the ability of certain drugs, such as doxorubicin (Dox), to kill tumor cells and concurrently induce antitumor immune responses triggered by dying tumor cells [8]. Molecular key events in Dox-induced ICD are the extracellular release of the high-mobility group 1 box (HMGB1) protein and the cell surface translocation of calreticulin (CRT) from the endoplasmic reticulum, where it exerts calcium-sensor and chaperone functions. These events trigger tumor cell phagocytosis by dendritic cells (DCs) and the subsequent DC-mediated recruitment of other immune subpopulations with antitumor activity [9,10]. Interestingly, MDR+ cells are often refractory to ICD [11] indicating that tumor cells can afford multiple strategies to survive and proliferate in the chemotherapy-treated host.

Zoledronic acid (ZA) is an aminobisphosphonate widely used in clinics to prevent bone resorption and treat bone disease in solid

tumors, including breast, prostate, lung cancer and multiple myeloma. ZA is a specific inhibitor of FPP synthase in the Mev pathway and exerts pleiotropic effects in tumor and non-tumor cells, such as osteoclasts, macrophages, endothelial cells and immune cells [12,13]. These effects are due to the intracellular deprivation of isoprenylated proteins and/or the accumulation of isopentenyl pyrophosphate which is exploited to activate V $\gamma$ 9V $\delta$ 2 T cells, a unique subset of unconventional T cells with regulatory and effector functions against microbes, stressed cells and tumor cells [14–16].

Previous data have shown that ZA enhances the anti-proliferative effect of Dox in drug-sensitive tumor cells [17,18] and clinical studies have been initiated in breast cancer patients to take advantage of this synergy [19]. However, it is currently unknown whether ZA has any impact on MDR and/or ICD in tumor cells. The aim of this study was two-fold: 1) to investigate the activity of the Mev pathway and Ras/RhoA-downstream signalling pathways in MDR $-$  and MDR $+$  tumor cells; 2) to evaluate the relationship, if any, between ZA-induced Mev pathway inhibition, Dox-induced cytotoxicity and ICD susceptibility. We found that a hyper-active Mev pathway is responsible for both chemo- and immune-resistance; thanks to the inhibition of Mev-pathway dependent signals, ZA restored Dox-induced cytotoxicity and ICD in MDR $+$  cells.

## Materials and Methods

### Chemicals

Fetal bovine serum (FBS) and culture medium were from Invitrogen Life Technologies (Carlsbad, CA). Plastic ware for cell cultures was from Falcon (Becton Dickinson, Franklin Lakes, NJ). ZA was a gift from Novartis (Basel, Switzerland). The specific inhibitors of farnesyl transferase FTI-277, geranylgeranyl transferase GGTI-286 and of RhoA kinase Y27632 were purchased from Calbiochem (San Diego, CA). Electrophoresis reagents were obtained from Bio-Rad Laboratories (Hercules, CA). The protein content of cell monolayers and lysates was assessed with the BCA kit from Sigma Chemical Co. (St. Louis, MO). Unless otherwise specified, all the other reagents were purchased from Sigma Chemical Co.

### Cell lines

Human colon cancer HT29, lung cancer A549, and breast cancer MCF7 are Dox-sensitive, MDR $-$  tumor cell lines (ATCC, Rockville, MD). Dox-resistant counterparts (HT29-dx, A549-dx and MCF7-dx) were generated by culturing parental cells in the presence of increasing concentrations of Dox for up to 20 passages [11,20,21]. For the present work, HT29-dx cells were grown in medium containing 250 nmol/L Dox, A549-dx cells in medium containing 100 nmol/L Dox, MCF7-dx cells in medium containing 0.5 nmol/L, and represented models of acquired MDR. The human hepatoma HepG2 cell line (ATCC) and the HP06 and HMM cancer cells were used as prototypic models of cells with a constitutive MDR phenotype and were previously described ([7,11,21]; in all these works HMM cells were named MM98 cells). Primary HP06 cells (gift of Prof. Anna Sapino, Department of Biomedical Sciences and Oncology, University of Torino, Italy) were derived from the peritoneal metastasis of a female patient with an invasive breast cancer, while primary HMM cells (Malignant Mesothelioma Biologic Bank, Azienda Ospedaliera Nazionale, Alessandria, Italy) were derived from the pleural effusion of a patient with histologically confirmed malignant mesothelioma, after written informed consent from the patients. The use of HP06 cells was approved by the Bioethics Committee

(“Comitato of Bioetica d’Ateneo”) of the University of Torino, Italy; the use of HMM cells was approved by the Bioethics Committee (“Comitato Etico Interaziendale”) of the “Azienda Ospedaliera Nazionale SS. Antonio e Biagio e Cesare Arrigo” of Alessandria, Italy. Primary cells were used at passages 2–4. All the cultures were supplemented with 10% FBS, 1% penicillin-streptomycin and 1% L-glutamine, and maintained in a humidified atmosphere at 37°C and 5% CO $_2$ .

### Intracellular Dox accumulation

Intracellular Dox contents were detected with a fluorimetric-based assay as reported [20] and expressed as nmol Dox/mg cell proteins according to a previously prepared calibration curve.

### Real-time polymerase chain reaction (RT-PCR)

Total RNA was extracted and reverse-transcribed using the QuantiTect Reverse Transcription Kit (Qiagen, Hilden, Germany). RT-PCR was carried out with IQ $^{\text{TM}}$  SYBR Green Supermix (Bio-Rad). The same cDNA preparation was used for the quantitation of *mdr1* gene, which encodes for human Pgp, and glyceraldehyde-3-phosphate dehydrogenase (GAPDH), chosen as a housekeeping gene. The sequences of *mdr1* primers were: 5'-TGCTGGAGCGGTTCTACG-3', 5'-ATAGGCAATGTTCT-CAGCAATG-3'. The sequences of GAPDH primers were: 5'-GAAGGTGAAGGTCGGAGT-3', 5'-CATGGTGAATCA-TATTGGAA-3'. The relative quantitation of each sample was performed by comparing the *mdr1* PCR product with the GAPDH PCR product with the Bio-Rad Software Gene Expression Quantitation.

### De novo synthesis of cholesterol and isoprenoids

Cells were labeled with 1  $\mu$ Ci/mL  $^3$ H-acetate (3600 mCi/mmol; Amersham Bioscience, Piscataway, NJ) and the synthesis of the radiolabeled cholesterol, FPP and GGPP was measured as described [22]. Results were expressed as pmol/mg cell proteins, according to the relative calibration curves.

### Ras and RhoA isoprenylation and activity

To detect the isoprenylated membrane-associated Ras or RhoA proteins and the non-isoprenylated cytosolic forms, cells were lysed in MLB buffer (125 mmol/L Tris-HCl, 750 mmol/L NaCl, 1% v/v NP40, 10% v/v glycerol, 50 mmol/L MgCl $_2$ , 5 mmol/L EDTA, 25 mmol/L NaF, 1 mmol/L NaVO $_4$ , 10  $\mu$ g/ml leupeptin, 10  $\mu$ g/ml pepstatin, 10  $\mu$ g/ml aprotinin, 1 mmol/L phenylmethylsulfonyl fluoride; pH 7.5) and centrifuged at 13 000 $\times$  g for 10 min at 4°C. An aliquot of supernatant was taken out for the Western blot of total Ras and RhoA, while the remaining part was centrifuged at 100 000 $\times$  g for 1 h at 4°C; both the supernatant (cytosolic extracts) and the pellet (membrane fractions) were solubilized in Laemli buffer (125 mmol/L Tris, 4% w/v SDS, 20% v/v glycerol and 1% w/v  $\beta$ -mercaptoethanol) and subjected to Western blotting, using an anti-Ras (Millipore, Billerica, MA) and an anti-RhoA (Santa Cruz Biotechnology Inc., Santa Cruz, CA) antibody. To evaluate Ras and RhoA activity, the GTP-bound fraction, taken as an index of active G-proteins [23] was measured, using a pull-down assay (with the Raf-1-GST fusion protein, agarose beads-conjugates, Millipore) and an ELISA assay (with the G-LISA $^{\text{TM}}$  RhoA Activation Assay Biochem Kit, Cytoskeleton Inc, Denver, CO), respectively, as described previously [22].

### RhoA kinase activity

RhoA kinase activity was evaluated with the CycLex Rho Kinase Assay Kit (CycLex Co., Nagano, Japan) following the manufacturer's instructions [22].

### Western blot analysis

Cells were lysed in MLB buffer, sonicated and centrifuged at  $13\,000\times g$  for 10 min at  $4^{\circ}\text{C}$ .  $10\ \mu\text{g}$  cell lysates were subjected to Western blotting and probed with the following antibodies: anti-phospho-(Thr202/Tyr204, Thr185/Tyr187)-ERK1/2 (Millipore); anti-ERK 1/2 (Millipore); anti-Hypoxia Inducible Factor-1 $\alpha$  (HIF-1 $\alpha$ ; BD Bioscience, San Jose, CA); anti-Pgp (Santa Cruz Biotechnology Inc.); anti-GAPDH (Santa Cruz Biotechnology Inc.), followed by the secondary peroxidase-conjugated antibodies (Bio-Rad). Proteins were detected by enhanced chemiluminescence (PerkinElmer, Waltham, MA).

To assess HIF-1 $\alpha$  phosphorylation, the whole cell lysate was immunoprecipitated with a polyclonal anti-HIF-1 $\alpha$  antibody (Santa Cruz Biotechnology Inc.), then probed for 1 h with a biotin-conjugated anti-phosphoserine antibody (Sigma Chemical Co.) followed by polymeric streptavidin-horseradish peroxidase-conjugates (Sigma Chemical Co.).

### HIF-1 $\alpha$ transcriptional activity

Nuclear proteins were extracted using the Nuclear Extract Kit (Active Motif, Rixensart, Belgium). The activity of HIF-1 on 10  $\mu\text{g}$  nuclear extracts was assessed with the TransAM<sup>TM</sup> HIF-1 Transcription Factor Assay Kit (Active Motif). For each set of experiments, blank (with double-distilled water), negative control (with mutated oligonucleotide) and competition assay (using 20 pmol of the wild type oligonucleotide with nuclear extracts of HMM cells grown at 3%  $\text{O}_2$  for 24 h) were included. In hypoxic conditions, the HIF-1 activity was  $257.53\pm 3.77$  mU/mg prot; in the competition assay, the corresponding HIF-1 activity was reduced to  $33.14\pm 1.39$  mU/mg prot ( $n=5$ ). The data were expressed as mU absorbance/mg cell proteins.

Chromatin Immunoprecipitation (ChIP) experiments to measure the binding of HIF-1 $\alpha$  on the "Hypoxia Responsive Element" of the *mdr1* promoter were performed as reported elsewhere [24].

### Cytotoxicity assay

Lactate dehydrogenase (LDH) activity was measured in the extracellular medium and in the cell lysate as described [20]. To measure the extracellular release of HMGB1, 20  $\mu\text{L}$  of the cells culture medium were boiled, resolved by SDS-PAGE and probe with an anti-HMGB1 antibody (Sigma Chemical Co.). Blots were pre-stained with Red Ponceau to check the equal loading of proteins. The ATP release was measured on 100  $\mu\text{L}$  of the cell culture medium with the ATP Bioluminescent Assay Kit (FL-AA, Sigma Aldrich Co.), using a Synergy HT Multi-Detection Microplate Reader (Bio-Tek, Winooski, VT). The results were expressed as nmol ATP/ml, according to the previously set titration curve.

### Analysis of cell surface CRT

Cells were incubated for 45 min ( $4^{\circ}\text{C}$ ) with an anti-CRT antibody (Affinity Bioreagents, Rockford, IL), as reported in [11] and analyzed using a FACS-Calibur system (BD Biosciences). For each analysis 100,000 events were collected. The percentage of CRT-fluorescent viable cells (propidium iodide-negative) was calculated with Cell Quest software (BD Biosciences). Control experiments included incubating cells with non-immune isotypic antibodies followed by the appropriate secondary antibody. Flow

cytometry results were confirmed by biotinylation assays [25], using the Cell Surface Protein isolation kit from Thermo Fisher Scientific Inc. (Rockford, IL). The entry of biotin in cells was excluded by checking the absence of cytosolic proteins (GAPDH, actin) in biotinylated extracts (not shown).

### Dendritic cell (DCs) generation and *in vitro* phagocytosis assay

DCs were generated from peripheral blood samples obtained from healthy donors kindly provided by the local Blood Bank (Fondazione Strumia, Torino, Italy), as previously reported [11]. Cells were harvested on day 6 and confirmed as immature DCs by morphology and immunophenotype.

MDR- HT29 and MDR+ HT29-dx and HMM cells were green-stained with PKH2-FITC (Sigma Chemical Co.), washed twice and incubated with a ratio of 1:1 for 18 h at  $37^{\circ}\text{C}$ . Co-cultures were then stained for 20 min at  $4^{\circ}\text{C}$  with APC-conjugated HLA-DR antibody (Miltenyi Biotec, Tetrow, Germany) to mark DCs. Two-color flow cytometry was performed with a FACScan cell sorter and CellQuest software (Becton Dickinson). At least 10,000 events were accumulated specifically backgating on DC morphology (region 1: FSC versus SSC). Tumor cell phagocytosis was assessed as the percentage of double-stained (FITC plus APC) cells. Tumor cells do not express significant amounts of HLA-DR, and they are excluded from region 1 by their morphology. In each set of experiments, a phagocytosis assay was performed by co-incubating DCs and tumor cells at  $4^{\circ}\text{C}$ , instead of  $37^{\circ}\text{C}$ , and the percentage of double-stained cells obtained after the incubation at  $4^{\circ}\text{C}$  was subtracted from values observed at  $37^{\circ}\text{C}$ . The phagocytosis rate was expressed as a phagocytic index, calculated as previously reported [9].

In fluorescence microscopy-based assays, PKH2-FITC green-stained tumor cells were incubated for 6 h or 24 h at  $37^{\circ}\text{C}$  with  $1\times 10^5$  DCs at a 1:1 ratio. Co-cultures were cytospun at  $1500\times g$  for 5 min onto glass slips, fixed with 4% w/v paraformaldehyde, washed and stained with a mouse polyclonal anti-MHCII antibody (Thermo Fisher Scientific Inc.). After washing, samples were incubated with an Alexa fluor 350-conjugated goat anti-mouse IgG antibody (Invitrogen) for 1 h at room temperature, washed, mounted with Gel Mount Aqueous Mounting and examined under a fluorescence microscope, as described above.

### DC-mediated CD8+ T-cell stimulation

After tumor cell phagocytosis, DCs were washed and co-cultured with autologous T cells, isolated from CD14-cells by immunomagnetic sorting with the Pan T Cell Isolation Kit (Miltenyi Biotec). DC and T cells were co-cultured for 10 days at a ratio of 1:5 in complete medium supplemented with IL-2 (10 U/mL). On day 10, CD107 expression on CD8+ T cells was determined by flow cytometry to determine the activation of tumor-specific cytotoxic T cells [26]. At least 100,000 events in the lymphocyte gate were acquired and analyzed by two-color flow cytometry. Tumor cell death induced by CD8+ T cells was also quantified by CFSE-labeling, measuring the percentage of HT29-dx cells double-positive for CFSE and propidium iodide as previously reported [14,15].

### Statistical analysis

All data in the text and figures are provided as means  $\pm$  SD. The results were analyzed by a one-way analysis of variance (ANOVA) with  $P<0.05$  as the significance cut-off. The  $r$  coefficient was calculated with Fig.P software (Fig.P Software Inc., Hamilton, Canada).

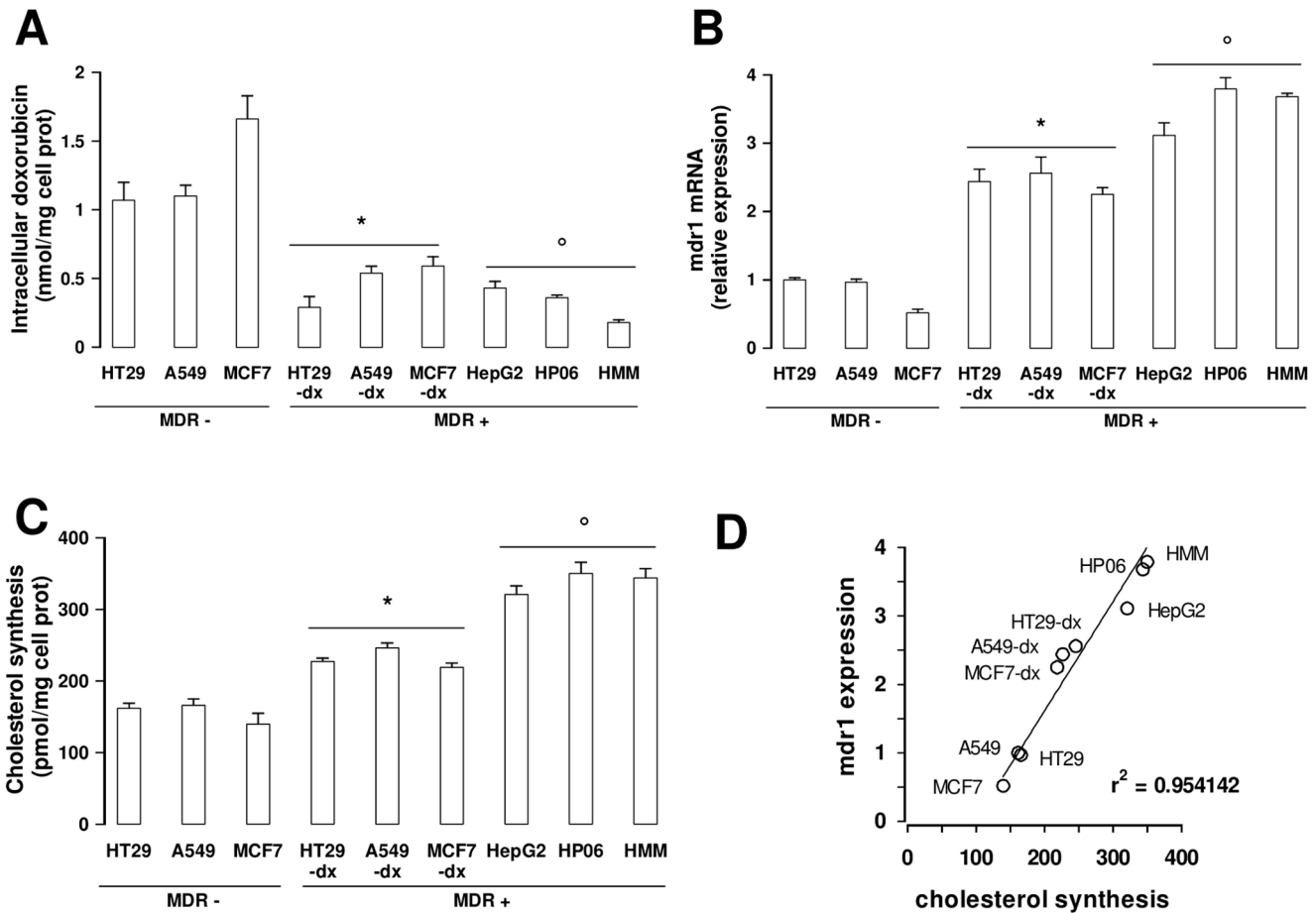


**Figure 1. Correlation between intracellular doxorubicin retention, *mdr1* expression and Mev pathway activity in MDR– and MDR+ tumor cells.** **A.** Intracellular doxorubicin (Dox) concentrations in MDR– cells (HT29, A549 and MCF7), in the corresponding acquired MDR+ counterparts (HT29-dx cells, A549-dx cells, MCF7-dx), and constitutive MDR+ cells (HepG2, HP06, HMM). Significantly lower concentrations were detected in cells with acquired MDR vs MDR– cells (HT29-dx vs HT29: \* $p < 0.002$ ; A549-dx vs A549: \* $p < 0.001$ ; MCF7-dx vs MCF7: \* $p < 0.001$ ), and in cells with constitutive MDR vs MDR– cells (mean value of intracellular doxorubicin in HepG2/HP06/HMM vs mean value in HT29/A549/MCF7:  $\circ p < 0.001$ ). **B.** *mdr1* mRNA expression. Significant higher *mdr1* levels were observed in cells with acquired MDR vs MDR– cells (HT29-dx vs HT29: \* $p < 0.002$ ; A549-dx vs A549: \* $p < 0.002$ ; MCF7-dx vs MCF7: \* $p < 0.001$ ), and in cells with constitutive MDR vs MDR– cells (mean value of *mdr1* levels in HepG2/HP06/HMM vs mean value in HT29/A549/MCF7:  $\circ p < 0.001$ ). **C.** Rate of cholesterol synthesis. Significant higher activity was measured in cells with acquired MDR vs MDR– cells (HT29-dx vs HT29: \* $p < 0.002$ ; A549-dx vs A549: \* $p < 0.002$ ; MCF7-dx vs MCF7: \* $p < 0.002$ ), and in cells with constitutive MDR vs MDR– cells (mean value of cholesterol synthesis in HepG2/HP06/HMM vs mean value in HepG2/HP06/HMM:  $\circ p < 0.001$ ). **D.** Direct correlation between the rate of cholesterol synthesis and the expression levels of *mdr1* in individual cell lines ( $r^2 = 0.95$ ). For panels **A**, **B**, and **C** bars represent the mean  $\pm$  SD of 3 independent experiments. doi:10.1371/journal.pone.0060975.g001

**Results**

**Correlation between *mdr1* expression and Mev pathway activity**

Intracellular Dox retention, *mdr1* mRNA levels, and cholesterol synthesis were measured as markers of Pgp activity, Pgp expression, and Mev pathway activity in HT29, A549, MCF7 cells (MDR– cells), HT29-dx, A549-dx, MCF7-dx cells (acquired MDR+ cells), and HepG2 cells, HP06, HMM cells (constitutive MDR+ cells), respectively. Both acquired and constitutive MDR+ cells retained significantly less Dox (Figure 1A) and showed higher *mdr1* mRNA levels (Figure 1B) than MDR– cells. Cholesterol synthesis was also significantly higher in MDR+ than in MDR– cells (Figure 1C). The differences between acquired and constitutive MDR+ cells were not statistically significant, even though the latter tended to retain less Dox, to express more *mdr1* mRNA

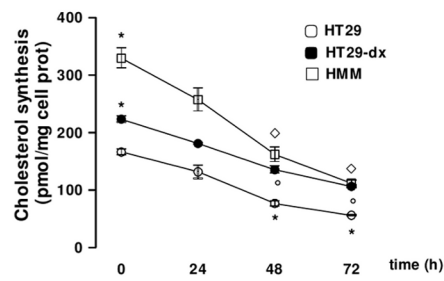
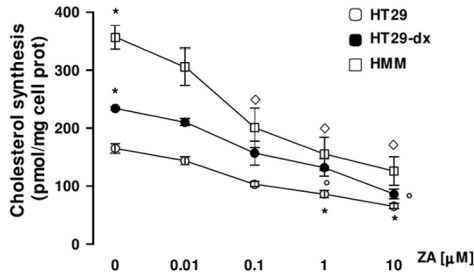
levels, and to generate more cholesterol than the former. A very significant correlation was observed between the rate of cholesterol synthesis and *mdr1* mRNA levels (Figure 1D).

**ZA inhibits Mev-dependent signalling pathways in MDR+ cells**

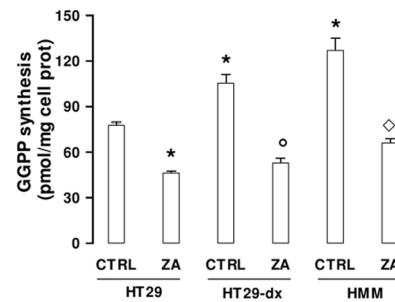
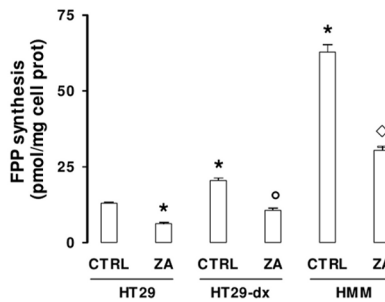
ZA was used to investigate the effect of Mev pathway inhibition in HT29, HT29-dx and HMM cells which were selected as prototypic models of MDR–, acquired MDR+ and constitutive MDR+ tumor cells respectively.

ZA induced a dose- (Figure 2A, left panel) and time-dependent (Figure 2A, right panel) decrease of cholesterol synthesis with a significant inhibition at 1  $\mu\text{mol/L}$  which was more evident in MDR+ HT29-dx and HMM cells than MDR– HT29 cells (Figure 2A). One  $\mu\text{mol/L}$  is also similar to the serum concentration observed in patients receiving ZA at clinically approved doses

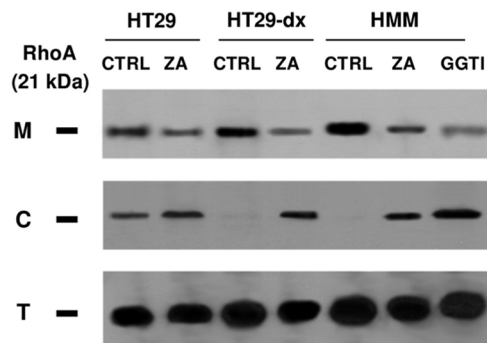
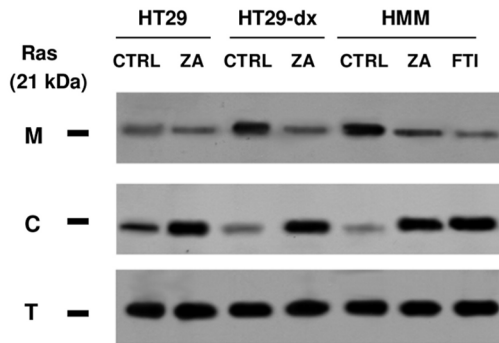
**A**



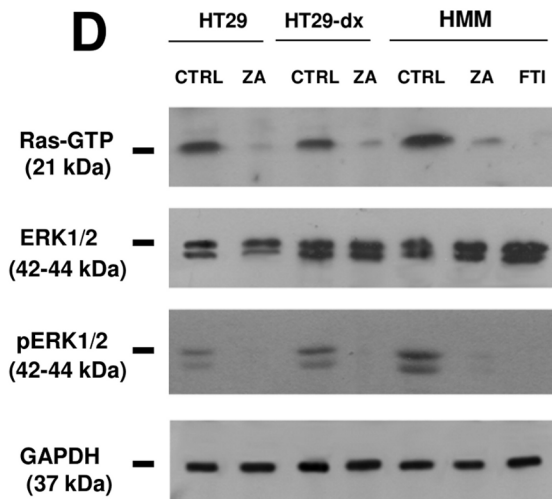
**B**



**C**



**D**



**E**

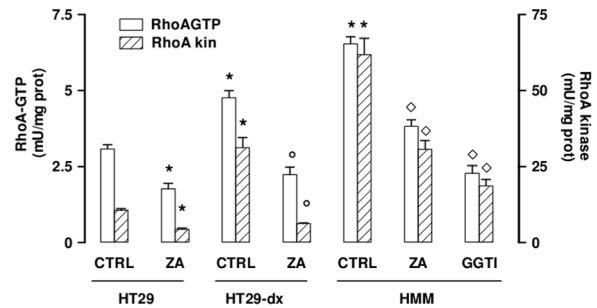


**Figure 2. Effects of ZA on cholesterol and isoprenoid synthesis, Ras/RhoA isoprenylation, and ERK1/2 and RhoA kinase activity in MDR<sup>-</sup> and MDR<sup>+</sup> cancer cells.** MDR<sup>-</sup> HT29, and MDR<sup>+</sup> HT29-dx and HMM cells were cultured without (CTRL) or with zoledronic acid (ZA). For panels B–E, ZA (1 μmol/L) was used for 48 h, FTI-277 (10 μmol/L, FTI), GGTI-286 (10 μmol/L, GGTI), Y27632 (10 μmol/L, Y276) for 24 h. **A. Left panel:** dose-dependent inhibition of cholesterol synthesis in cells treated with 0.01–10 μmol/L ZA for 24 h. Inhibition was statistically significant in HT29 (\*p<0.001), HT29-dx (°p<0.01) d HMM cells (◊p<0.005) vs baseline values (0). **Right panel:** time-dependent inhibition of cholesterol synthesis in cells treated with 1 μmol/L ZA for 24–72 h. Inhibition was statistically significant in HT29 (\*p<0.001), HT29-dx (°p<0.0001) and HMM cells (◊p<0.001) vs baseline values (0). For both panels: HT29-dx/HMM vs HT29: \*p<0.001. **B.** MDR<sup>+</sup> cells synthesized higher amounts of FPP (left panel) and GGPP (right panel) than MDR<sup>-</sup> cells (\*p<0.005). ZA significantly lowered FPP synthesis vs untreated (CTRL) cells (HT29: \*p<0.001; HT29-dx: °p<0.002; HMM: ◊p<0.001) and GGPP synthesis vs untreated (CTRL) cells (HT29:\*p<0.02; HT29-dx: °p<0.001; HMM:◊p<0.005). **C.** MDR<sup>+</sup> cells displayed an unbalanced distribution between isoprenylated membrane-bound (M) and non isoprenylated cytosolic (C) Ras (left panel) and RhoA (right panel) compared with MDR<sup>-</sup> cells. ZA treatment increased the amount of cytosolic Ras and RhoA. T: amount of Ras and RhoA in whole cell lysates. **D.** ZA decreased Ras activity, measured as Ras-GTP amount, and phospho-(Thr202/Tyr204, Thr185/Tyr187)-ERK1/2 amount. GAPDH data are shown to confirm equivalent protein loading. **E.** MDR<sup>+</sup> cells had significantly higher amounts of RhoA-GTP (open bars) and RhoA kinase (hatched bars) than MDR<sup>-</sup> cells (\*p<0.005); ZA decreased both RhoA-GTP and RhoA kinase vs untreated (CTRL) cells (HT29-dx: °p<0.02; HMM:◊p<0.02). The results shown in panels C and D are representative of 3 experiments. In panels A, B, and E the results represent the mean ± SD of 3 experiments. doi:10.1371/journal.pone.0060975.g002

[27,28] and therefore this concentration was used throughout the study.

According to the hyper-active Mev pathway, MDR<sup>+</sup> HT29-dx and HMM cells showed higher FPP (Figure 2B, left panel) and GGPP (Figure 2B, right panel) synthesis than MDR<sup>-</sup> HT29 cells. Both MDR<sup>-</sup> and MDR<sup>+</sup> cells had detectable amounts of isoprenylated, membrane-bound Ras and non-isoprenylated, cytosolic Ras, although the former was largely predominant in MDR<sup>+</sup> cells as a consequence of the increased FPP supply favoring Ras isoprenylation (Figure 2C, left panel). Membrane-bound and cytosolic RhoA also showed a similar pattern in MDR<sup>+</sup> HT29-dx and HMM vs MDR<sup>-</sup> HT29 cells as a consequence of the increased GGPP production and RhoA isoprenylation (Figure 2C, right panel).

The excess of membrane-bound Ras and RhoA resulted in increased activity of the corresponding downstream signalling pathways: intracellular levels of GTP-bound Ras (Figure 2D), a marker of Ras activation, and ERK1/2 phosphorylation (Figure 2D), as well as the amounts of GTP-bound RhoA (Figure 2E) and the activity of RhoA kinase (Figure 2E) were higher in MDR<sup>+</sup> HT29-dx and HMM cells than MDR<sup>-</sup> HT29 cells.

ZA treatment abrogated the differences between MDR<sup>-</sup> and MDR<sup>+</sup> cells. By inhibiting FPP and GGPP synthesis (Figure 2B), ZA decreased the amounts of membrane-bound Ras and RhoA (Figure 2C), intracellular Ras-GTP and RhoA-GTP contents, and the activity of their downstream signalling pathways (Figure 2D–E). These effects were more evident in MDR<sup>+</sup> HT29-dx and HMM cells than MDR<sup>-</sup> HT29 cells according to their Mev pathway activity.

### ZA decreases Pgp expression by reducing HIF-1α activation via Ras/ERK1/2- and RhoA/Rho-A kinase downregulation

HIF-1α, a master regulator of several genes including *mdr1* [29], can become constitutively activated even under normoxic conditions upon serin phosphorylation by RhoA kinase [30] and MAP kinases [31]. Phosphorylated (pHIF-1α) and non-phosphorylated HIF-1α were undetectable by Western blot in MDR<sup>-</sup> HT29 cells, whereas both pHIF-1α and HIF-1α were expressed in MDR<sup>+</sup> HT29-dx and HMM cells (Figure 3A). HIF-1α was transcriptionally active in MDR<sup>+</sup> cells, as shown by the significantly higher amounts of nuclear HIF-1 bound to its specific DNA target sequence (Figure 3B). ZA had no effect on MDR<sup>-</sup> cells, whereas it reduced the amount of pHIF-1α and lowered total HIF-1α levels and activity in MDR<sup>+</sup> cells (Figure 3A–B).

HIF-1α was constitutively bound to the Hypoxia Response Element of the *mdr1* promoter in MDR<sup>+</sup> cells HT29-dx and

HMM cells, but not in MDR<sup>-</sup> HT29 cells (Figure 3C). This explains why the expression of the Pgp protein was only detectable in MDR<sup>+</sup> cells (Figure 3D) and why these cells showed significantly lower Dox retention than MDR<sup>-</sup> cells (Figure 3E).

ZA treatment effectively abrogated HIF-1α-binding to the *mdr1* promoter (Figure 3C) and Pgp expression (Figure 3D), and significantly increased intracellular Dox levels in MDR<sup>+</sup> HT29-dx and HMM cells which became comparable to those observed in MDR<sup>-</sup> HT29 cells (Figure 3E). Intracellular Dox retention in MDR<sup>+</sup> cells was significantly increased when ZA was administered before Dox, but neither *vice versa*, nor when the two drugs were used together (Figure S1).

To provide further evidence that the ZA-induced Pgp down-regulation in MDR<sup>+</sup> cells was dependent on pHIF-1α suppression via ERK1/2 and RhoA kinase inhibition, side-by-side experiments were performed in the presence of specific inhibitors of ERK1/2 kinases (PD98059), RhoA kinase (Y27632) and HIF-1 (YC-1). In MDR<sup>+</sup> HMM cells these inhibitors showed the same effects of ZA in terms of pHIF-1α levels (Figure 4A), HIF-1 transcriptional activity (Figure 4B), Pgp expression (Figure 4C), and Dox retention (Figure 4D).

Altogether, these data confirm that targeting the Mev pathway in MDR<sup>+</sup> cells abrogates Pgp expression and promotes Dox retention by inhibiting the Ras/ERK1/2/HIF-1α/*mdr1* and the RhoA/RhoA kinase/HIF-1α/*mdr1* pathways.

### ZA restores Dox-induced cytotoxicity and ICD in MDR<sup>+</sup> cells

We then investigated whether the increased ZA-induced Dox retention was sufficient to induce cytotoxicity and ICD in MDR<sup>+</sup> cells.

The release of intracellular LDH was used to assess Dox-induced cytotoxicity (Figure 5A). Dox alone sufficed to induce a significant cytotoxicity in MDR<sup>-</sup> HT29 cells, while ZA alone had no activity and did not increase Dox cytotoxicity when used in combination. On the contrary, MDR<sup>+</sup> HT29-dx and HMM cells were resistant to Dox alone, but they became more vulnerable when Dox was used after ZA treatment (Figure 5A).

Hallmarks of ICD are the extracellular release of HMGB1 and ATP, and the translocation of CRT from the cytoplasm to the cell surface [10,32]. Neither MDR<sup>-</sup> nor MDR<sup>+</sup> cells showed detectable amounts of HMGB1 in the supernatants under baseline conditions or after ZA treatment (Figure 5B). Likewise, the release of ATP (Figure 5C) and the amount of cell surface CRT (Figure 5D) were low and not significantly different under baseline conditions or after ZA treatment in both MDR<sup>-</sup> and MDR<sup>+</sup> cells.

Dox alone was sufficient to induce the release of HMGB1 and ATP, and CRT translocation in MDR<sup>-</sup> HT29 cells and these effects were not further enhanced by ZA treatment (Figure 5B–D). On the contrary, while MDR<sup>+</sup> HT29-dx and HMM cells were

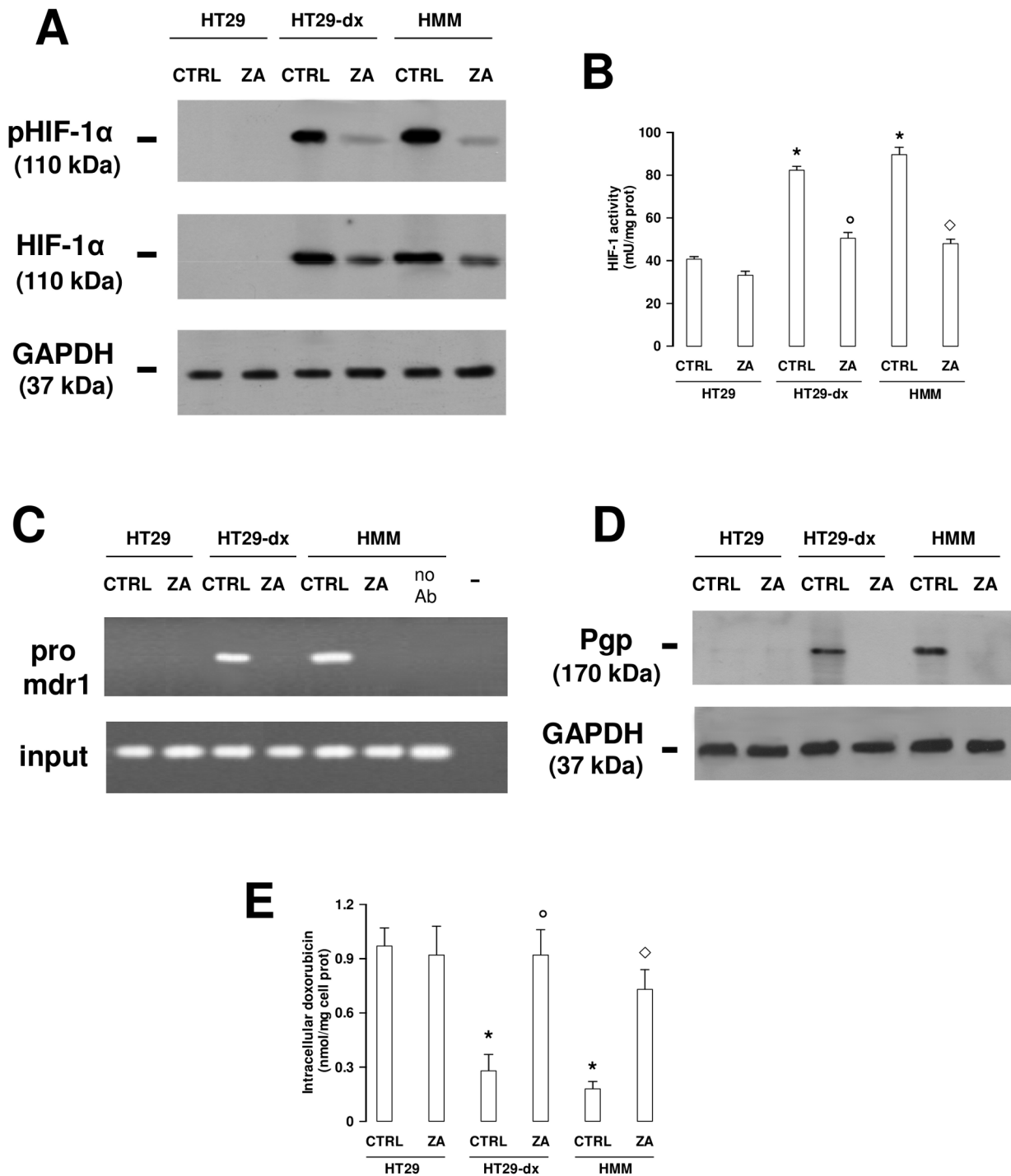


**Figure 3. ZA-induced inhibition of HIF-1α activity and Pgp expression in MDR+ cancer cells.** **A.** Detection of phosphorylated (pHIF-1α) and total HIF-1α in MDR- HT29, and MDR+ HT29-dx and HMM cells after 48-hour incubation without (CTRL) or with 1 μmol/L ZA (ZA). **B.** HIF-1 activity was higher (\*p<0.001) in MDR+ HT29-dx and HMM cells than HT29 cells. After ZA treatment (as reported in **A**), a significant decrease of HIF-1 activity was observed in HT29-dx (°p<0.001) and HMM cells (◇p<0.001). **C.** Chromatin immunoprecipitation of HIF-1α on *mdr1* promoter in MDR- and MDR+ cells, treated as reported in **a**. *pro mdr1*: PCR product from immunoprecipitated samples. *Input*: PCR product from non immunoprecipitated samples (genomic DNA). *no Ab*: samples incubated in the absence of anti-HIF-1α antibody. “-”: blank. **D.** Western blotting detection of Pgp in cells treated as described in **A**. **E.** Intracellular doxorubicin was measured spectrofluorimetrically: significantly lower concentrations were detected in HT29-dx and HMM vs HT29 cells (\*p<0.002), significantly higher concentrations in ZA-treated cells vs untreated (CTRL) counterparts (HT29-dx: °p<0.02; HMM: ◇p<0.02). The results shown in panels **A**, **C** and **D** are representative of 3 experiments. For panels **B** and **E** the bars represent the mean ± SD of 3 independent experiments. doi:10.1371/journal.pone.0060975.g003

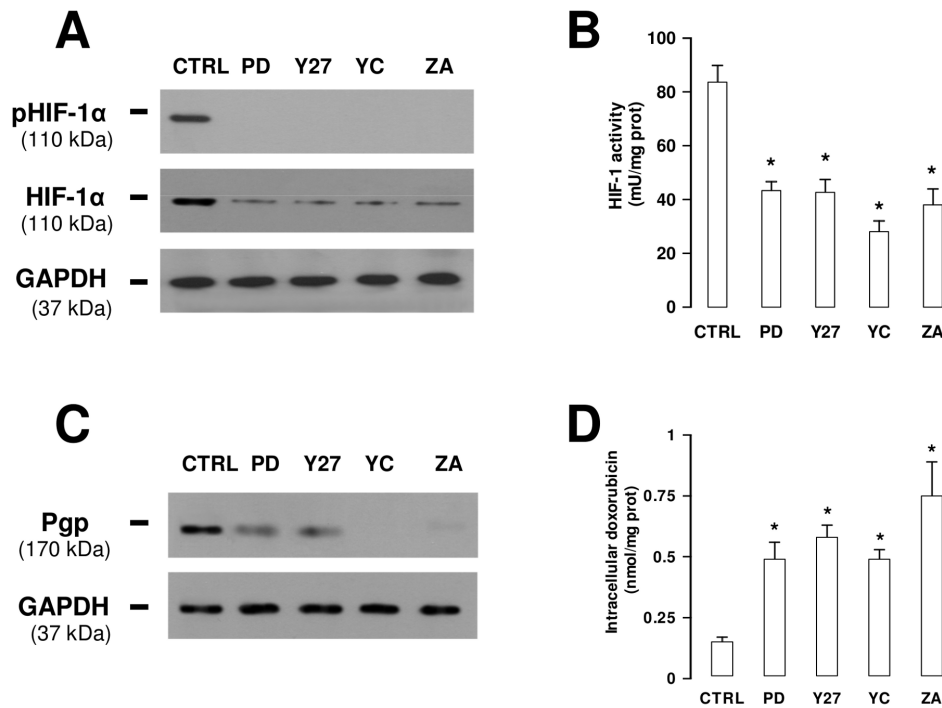


**Figure 4. Effects of ZA and inhibitors of ERK1/2, RhoA kinase, HIF-1 $\alpha$  on MDR+ cells.** **A.** Phospho(Ser)-HIF-1 $\alpha$  (pHIF-1 $\alpha$ ) and total HIF-1 $\alpha$  expression in HMM cells left untreated (CTRL) or treated for 24 h at 10  $\mu$ mol/L with the ERK1/2 kinase inhibitor PD98059 (PD), RhoA kinase inhibitor Y27632 (Y27), HIF-1 $\alpha$  inhibitor YC-1 (YC), and 1  $\mu$ mol/L ZA for 48 h. GAPDH data are shown to confirm equivalent per lane protein loading. **B.** HIF-1 activity in HMM cells left untreated (CTRL) or treated as reported in panel **A**. All differences between treated vs untreated cells are statistically significant (\*  $p < 0.01$ ). **C.** Pgp expression in HMM cells of untreated (CTRL) and treated as reported in panel **A**. **D.** Intracellular doxorubicin concentrations in HMM cells in cells incubated as reported above in medium alone (CTRL), followed by 1  $\mu$ mol/L Dox for a further 24 h. Differences between treated vs untreated cells are statistically significant (\* $p < 0.01$ ). Results shown in panels **A** and **C** are representative data from one of 2 experiments. For panels **B** and **D**, the results represent the mean  $\pm$  SD of 3 independent experiments. doi:10.1371/journal.pone.0060975.g004

refractory to Dox alone, they released HMGB1 (Figure 5B) and ATP (Figure 5C), and showed CRT translocation (Figure 5D) after ZA+Dox treatment. CRT translocation was confirmed with a biotinylation assay in both MDR $-$  and MDR+ cells (Figure S2).

These results indicate that the increased Dox retention induced by ZA treatment is sufficient to induce tumor cell cytotoxicity and to promote ICD of MDR+ cells.

### ZA enhances the phagocytosis of MDR+ tumor cells by DCs and induces the generation of tumor-specific CD8+ T cells

Next, we investigated whether ICD triggered by ZA+Dox could be sensed by the immune system via DCs [10,32]. As expected, both untreated or ZA-treated tumor cells were poorly phagocytosed by DCs, with MDR+ cells being more resistant than MDR $-$  cells (Figure 6A). Dox alone was sufficient to induce the phagocytosis of MDR $-$  HT29 cells which was further enhanced by ZA treatment. By contrast, Dox alone was unable to induce MDR+ HT29-dx and HMM cell phagocytosis. However, when Dox was used in combination with ZA, MDR+ cells became recognizable by DCs and significant phagocytosis was detected in MDR+ cells (Fig. 6 Figure 6A). Multiple cell-to-cell contact sites were established after 6 hours incubation of DCs with ZA+Dox-treated MDR+ HT29-dx cells, and clear evidence of internalization was documented after 24 hours (Figure 6B).

Next, we investigated whether the phagocytosis of ZA+Dox-treated MDR+HT29-dx cells increased the immunostimulatory capacity of DCs. The highest CD86 expression, a marker of DC

maturation, was observed in DCs exposed to ZA+Dox-treated MDR+ HT29-dx cells (Figure S3) and this resulted in a better capacity to activate autologous cytotoxic CD8+ T cells. Cytofluorometric analysis of cell surface CD107 expression on CD8+ cells was used as a surrogate marker of antigen-specific cytotoxic T-cell activation (Figure 6C–D). An increase of CD8+ CD107+ cells was observed after a 10-day incubation of T cells with autologous DCs loaded with MDR+ HT29-dx cells treated with ZA+Dox. The flow cytometry of a representative experiment is shown in Figure 6C, while pooled data from 4 experiments are given in Figure 6D. T cells incubated with DC exposed to ZA+Dox-treated MDR+ HT29-dx cells also showed increased cytotoxic activity against untreated MDR+ HT29-dx cells (Figure S4).

### Discussion

Constitutive and/or acquired MDR is a major obstacle to successful anti-tumor chemotherapy and the development of safe and effective MDR-reversing agents remains an unmet clinical need. In this study, we investigated whether the Mev pathway is involved in MDR and is eventually targetable for therapeutic intervention.

We initially analyzed the Mev pathway activity in a panel of MDR $-$ , acquired MDR+ and constitutive MDR+ cancer cells. The latter uniformly showed significantly higher Mev pathway activity than MDR $-$  cells, probably reflecting an increased transcription of 3-hydroxy-3-methylglutaryl-CoA reductase, the pace-maker enzyme in the Mev pathway. Indeed, 3-hydroxy-3-

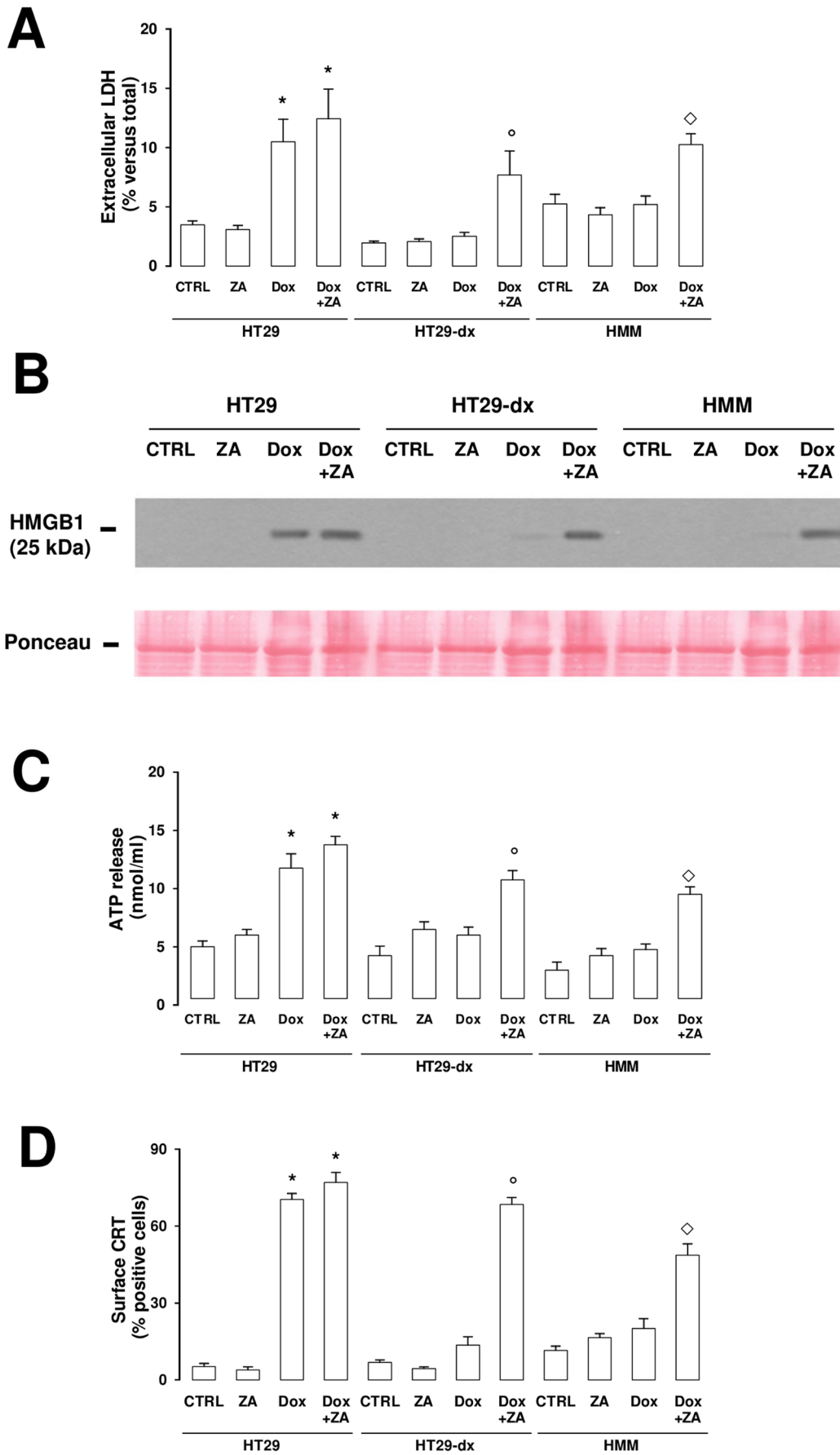


**Figure 5. ZA restores doxorubicin-induced cytotoxicity and ICD in MDR+ tumor cells.** MDR− HT29 and MDR+ HT29-dx, and HMM cells were incubated for 48 h without (CTRL) or with 1 μmol/L ZA, for 24 h with 1 μmol/L Dox, for 48 h with 1 μmol/L ZA, followed by 1 μmol/L Dox for additional 24 h (ZA+Dox). **A.** LDH release. Dox alone and ZA+Dox induced a significant cytotoxicity in HT29 cells (\* $p < 0.005$ ). ZA+Dox induced a significant increase of cytotoxicity in HT29-dx ( $p < 0.05$ ) and HMM cells ( $p < 0.02$ ). **B.** Western blot analysis of extracellular HMGB1. Dox alone and ZA+Dox in HT29 cells, ZA+Dox in HT29-dx and HMM cells induced the release of HMGB1 in the cell culture medium. Red Ponceau staining was used to check the equal loading of proteins. **C.** Extracellular release of ATP. Dox and ZA+Dox induced a significant increase of extracellular ATP in HT29 cells (\* $p < 0.01$ ). ZA+Dox elicited a significant release of ATP in HT29-dx ( $p < 0.002$ ) and HMM cells ( $p < 0.001$ ). **D.** Cell surface CRT exposure. Dox and ZA+Dox induced a significant CRT exposure in HT29 cells (\* $p < 0.001$ ). ZA+Dox induced a significant CRT exposure in HT29-dx ( $p < 0.001$ ) and HMM cells ( $p < 0.005$ ). For panels **A**, **C** and **D** bars represent the mean  $\pm$  SD of 3 independent experiments. For panel **B** the results are representative data from one of 2 experiments.

doi:10.1371/journal.pone.0060975.g005

methylglutaryl-CoA reductase is under the transcriptional control of the sterol regulated element binding protein-2, which is regulated by intracellular sterol levels, and by transcription factors such as HIF-1 $\alpha$  [33], which can be constitutively activated in MDR+ tumor cells [34] (see also below).

Increased intracellular cholesterol levels can contribute to MDR by facilitating the localization and functional activation of Pgp in the plasma membrane [5,21,35]. Although the existence of a correlation between cholesterol levels and Pgp expression has previously been postulated [36,37], there is yet to be a molecular or metabolic linkage. Here we show the existence of a correlation between the rate of cholesterol synthesis and *mdr1* levels, indicating that the Mev pathway activity can directly regulate Pgp expression.

To further document this relationship, we targeted the Mev pathway with ZA, a selective FPPS inhibitor. ZA induced a significant decrease of cholesterol, FPP and GGPP synthesis which was more pronounced in MDR+ than in MDR− cells, according to the higher baseline Mev pathway activity in the former. Notably, ZA produced these effects at 1 μmol/L which is a clinically compatible concentration [13,17,28]. After intravenous administration, ZA avidly impregnates the bone mineralized component, where it reaches long-lasting millimolar concentrations, but levels around 1 μmol/L are also detectable for several hours in the peripheral blood [17,38].

Intermediate metabolites of the Mev pathway are the isoprenoids FPP and GGPP, which are necessary for the isoprenylation and activity of the small GTPases Ras and RhoA. We enquired whether Ras and/or Rho-dependent signals were involved in the linkage between the Mev pathway, *mdr1* expression and Pgp activity. Isoprenylated active Ras and RhoA GTPases were detectable in both MDR− and MDR+ cells, but much more abundantly expressed in the latter. By limiting isoprenoid supply, ZA decreased Ras and RhoA isoprenylation, increased the ratio between inactive cytosolic GTPase and active membrane-associated GTPase, reduced the GTP-binding capacity and impaired Ras and RhoA interactions with their downstream effectors ERKs and RhoA kinases. MDR+ cells were apparently more susceptible to ZA effects, most likely because they had a higher baseline rate of Mev pathway activity and are therefore more susceptible to the shortage of isoprenoid supply generated by ZA-induced Mev pathway inhibition. Under this perspective, a high Mev pathway activity should be considered not only as a marker of tumor aggressiveness and poor prognosis [2,3], but also as a potential therapeutic target implying a “collateral sensitivity” of MDR tumors [39].

A striking difference between MDR− and MDR+ cells was the amount of intracellular HIF-1 $\alpha$ , one of the downstream targets of ERK1/2 and RhoA kinase [30,31]. The  $\alpha$  subunit of HIF undergoes proteasomal degradation under normoxic conditions unless stabilized by serine phosphorylation. Under basal conditions, HIF-1 $\alpha$  and Pgp, which is upregulated by HIF-1 $\alpha$  [29], were undetectable in MDR− cells, whereas they were highly expressed in MDR+ cells with a higher Mev pathway activity. ZA significantly decreased both pHIF-1 $\alpha$  and non-phosphorylated

HIF-1 $\alpha$  expression, abrogated HIF-1 $\alpha$ -driven Pgp expression, and increased intracellular Dox retention in MDR+ cells to similar levels of MDR− cells.

Altogether, these data indicate that the Mev-pathway dependent Ras/ERK1-2 and RhoA/RhoA kinase axes promote the phosphorylation and nuclear translocation of HIF-1 $\alpha$  in MDR+ cells where it induces the transcriptional activation of the *mdr1* gene leading to Pgp expression and Dox extrusion. This hypothesis was further validated by the demonstration in HMM MDR+ cells that both ZA and the ERK1/2, RhoA kinase and HIF-1 $\alpha$  inhibitors decreased Pgp expression and increased intracellular Dox concentrations. To the best of our knowledge, this is the first report demonstrating that the Mev pathway can regulate HIF-1 $\alpha$  transcriptional activity. These data also provide a biochemical explanation to the recent observation that ERK1/2 increases the expression of membrane efflux pumps and Dox resistance in malignant mesothelioma [40].

MDR reversion occurs when Dox reaches a critical intracellular concentration sufficient to elicit direct cytotoxicity. Indeed, ZA significantly increased Dox-induced cytotoxicity in MDR+ HT29-dx and HMM cells indicating that the intracellular drug concentration had exceeded the critical threshold. Previous studies have reported a synergistic activity of ZA and Dox in breast cancer cell lines [18,41]. This synergy was observed only when tumor cells were treated with Dox for 24 hours before ZA exposure. In our experiments, the highest intracellular accumulation of Dox was achieved in MDR+ cells if ZA treatment preceded Dox exposure. Even though this discrepancy might well be due to the different cell type and experimental conditions, it is reasonable from the biochemical standpoint that the synergy between ZA and Dox is enhanced if exposure to the latter is preceded by Mev pathway inhibition to trigger the cascade of events ultimately leading to Pgp down-regulation. These data suggest that targeting the Mev pathway may be exploited as a priming strategy to restore chemosensitivity in MDR+ cells.

In addition to killing cancer cells directly, some classes of chemotherapeutic drugs are endowed with unexpected immune activating properties [10]. These drugs trigger “danger signals” and “danger associated molecular patterns” from dying tumor cells which stimulate innate and adaptive immune responses [42]. Dox is a prototypic drug that induces ICD, whose hallmarks are the release of HMGB1 protein and ATP in the supernatant, and the translocation of CRT from the endoplasmic reticulum to the plasma membrane [32]. HMGB1 and CRT are sensed by dendritic cells (DCs) as an “eat me” signal, promoting tumor cell phagocytosis and cytotoxic T-cell activation [9,10,32].

Interestingly, it has been proposed that tumor cells that are resistant to direct chemotherapy-induced cytotoxicity are also have a tendency to escape ICD. A possible mechanism is the inadequate intracellular Dox retention in MDR+ cells which does not exceed the critical threshold to elicit CRT translocation [11]. Moreover, we, and others, have suggested that Pgp may have an immunosuppressive role by interfering with CRT functional activity [25,43].

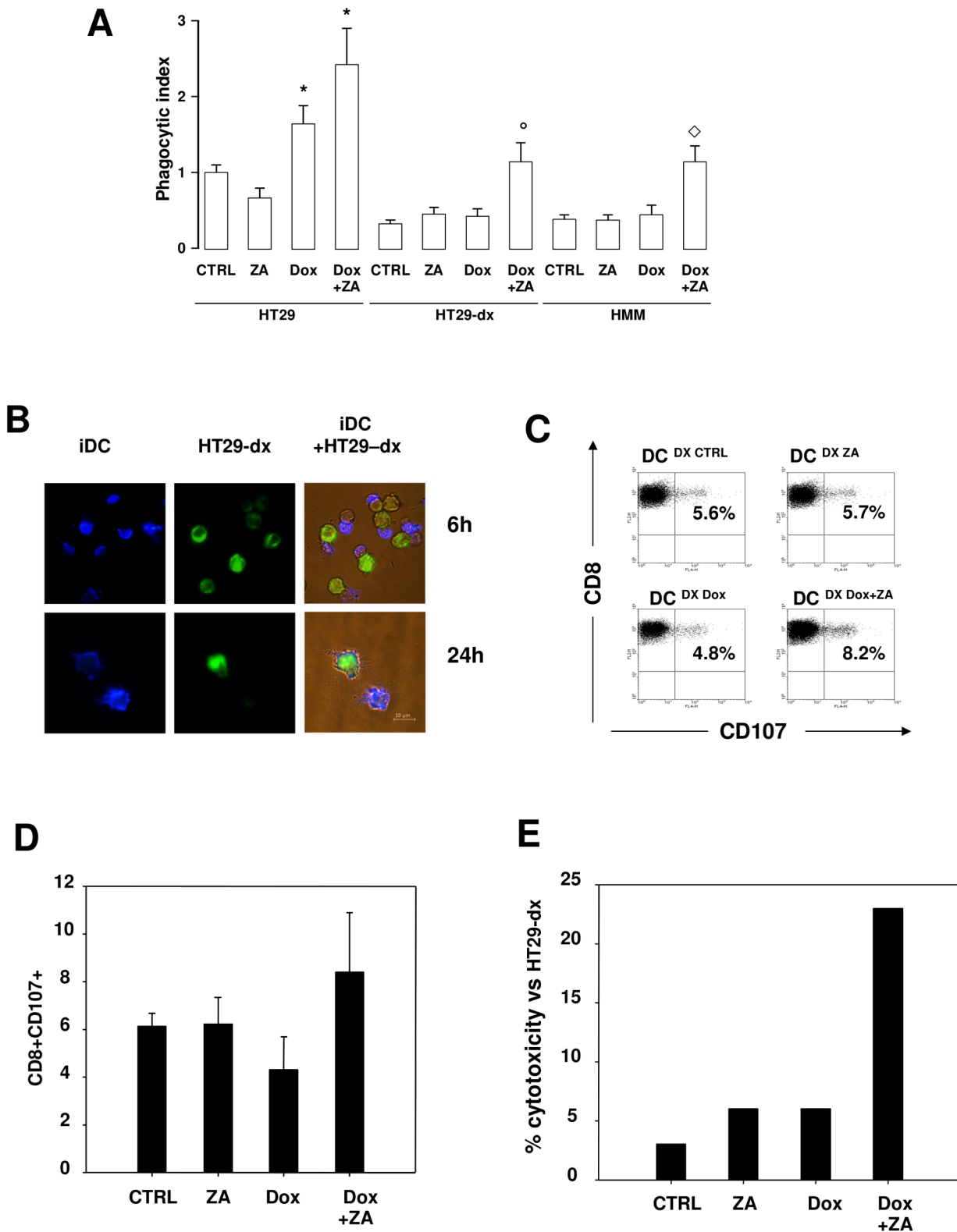


**Figure 6. ZA increases the internalization of MDR+ cells by autologous DCs and the subsequent activation of cytotoxic CD8+ T cells.** **A.** DC-mediated internalization of HT29, HT29-dx, and HMM cells after incubation with ZA and/or Dox. Tumor cells were incubated for 48 h without (CTRL) or with 1 μmol/L ZA, for 24 h with 1 μmol/L Dox, for 48 h with 1 μmol/L ZA, followed by 1 μmol/L Dox for additional 24 h (ZA+Dox). Dox alone and ZA+Dox significantly increased internalization of HT29 cells (\*p<0.02). ZA+Dox increased internalization of HT29-dx (°p<0.005) and HMM (°p<0.005) cells. Results represent the mean ± SD of 3 independent experiments. **B.** Fluorescence microscopy analysis of HT29-dx internalization after 6 and 24 h incubation with DCs. HT29-dx cells were incubated with ZA+Dox as reported in A. Micrographs are from one representative of 3 experiments. **C.** Cytotoxic activation of CD8+ T cells after 10 days incubation of purified T cells with autologous DCs pulsed with HT29-dx tumor cells,

treated as reported in a. Cytofluorometric analysis of cell surface CD107 expression was used as a marker of specific TCR-induced CD8+ T-cell degranulation. Results are from one representative of 4 experiments. **D.** Pooled data of CD107 expression on CD8+ T cells after incubation with autologous DC as reported above. Bars represent the mean  $\pm$  SEM of 4 experiments. doi:10.1371/journal.pone.0060975.g006

This work confirms the close relationship between MDR and ICD. As expected, direct cytotoxicity and ICD occurred jointly in Dox-treated MDR- HT29 cells that showed the release of extracellular LDH, an index of direct cell damage and necrosis, concurrently with the release of extracellular HMGB1 and ATP, and CRT translocation. These events culminated in the phagocytosis of Dox-treated MDR- HT29 cells by DCs and the induction of antigen-specific cytotoxic CD8+ cells. This immunogenic sequence was only minimally increased by concurrent ZA treatment. By contrast, the insufficient Dox retention in MDR+ HT29-dx and HMM cells did not induce any significant extracellular LDH and ATP release or any CRT translocation. This allowed MDR+ cells to escape DC recognition and phagocytosis and antigen-specific CD8+ T cells were not generated by DC exposed to Dox-treated MDR+ HT29-dx cells. Of note, susceptibility to ICD was restored when MDR+ cells were treated with ZA and Dox, probably because intracellular Dox retention was increased as a consequence of Pgp down-modulation. Under these conditions, MDR+ cells were sensed and

effectively phagocytised by DC which increased the expression of activation markers such as CD86 and induced the generation of cytotoxic CD8+ T lymphocytes. Although we cannot exclude that ZA enhances the cytotoxicity of DOX in MDR+ cells with additional mechanisms, it is noteworthy that it is able to reinstate an ICD in previously refractory cells. Compared to other MDR-reversing agents [44,45], ZA showed the unique property to combine the ability to improve chemotherapy-induced cytotoxicity with the capacity to promote chemotherapy-induced immunogenic cell death. This “multi-target” activity reinstates a complete chemosensitivity in MDR+ cells.

**Conclusions**

In conclusion, we propose that the hyper-activity of the Mev pathway is a metabolic signature of MDR+ cells and a common denominator linking the resistance to chemotherapy, due to the increased drug efflux and to the resistance to the pro-immunogenic effects of chemotherapy (Figure 7A). However, this hyper-

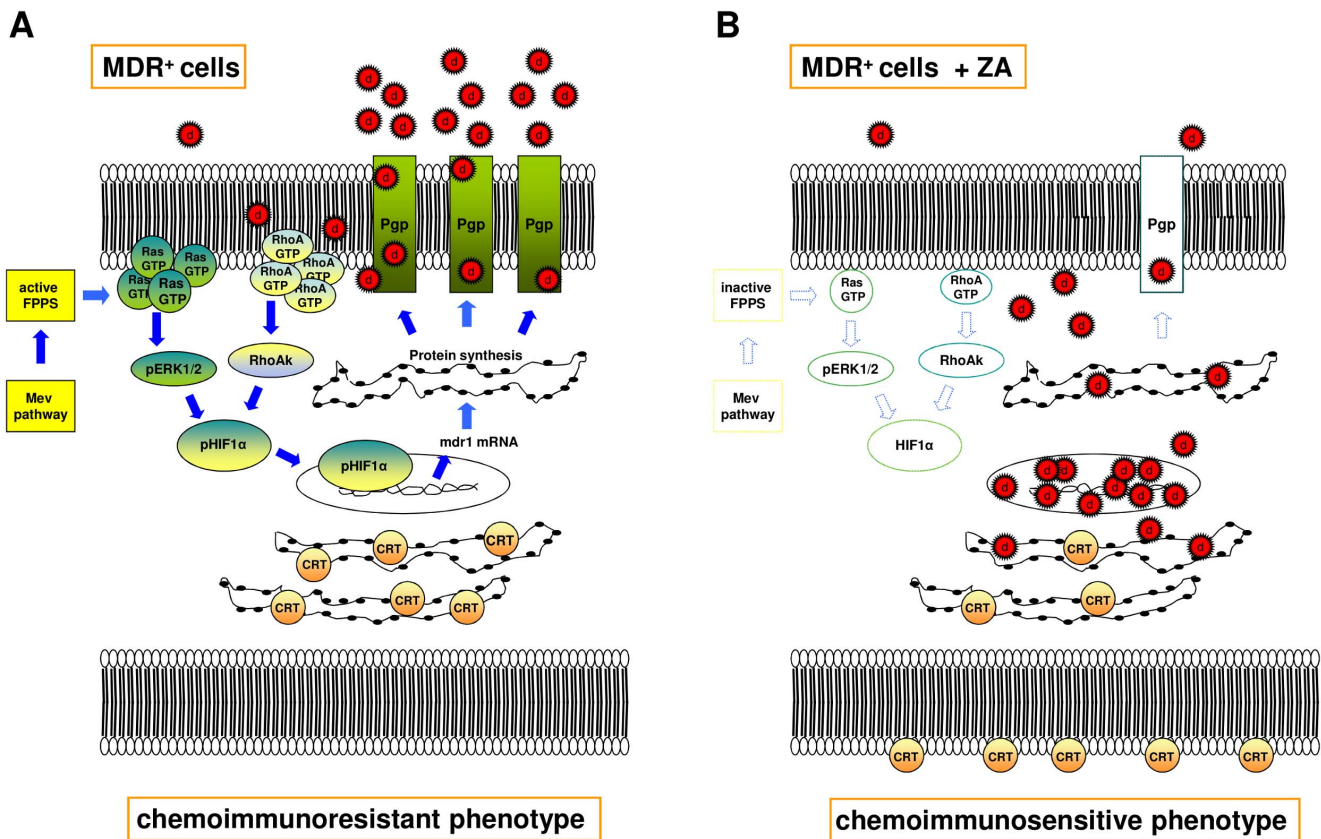


**Figure 7. Schematic drawing of mechanisms operated by ZA to reverse chemoresistance and immune-resistance.** **A.** The accelerated Mev pathway in MDR+ cells leads to the constitutive activation of Ras/ERK1-2 and RhoA/RhoA kinase downstream signalling pathways which culminates into HIF-1 $\alpha$  activation and plasma membrane Pgp expression. The higher amounts of plasma membrane-associated cholesterol in MDR+ cells also contribute to the functional Pgp activation. The higher efficiency to extrude Dox protects MDR+ cells from cytotoxicity and ICD epitomized by CRT exposure on the cell surface. **B.** By inhibiting the Mev pathway, ZA downregulates the Ras/ERK1-2 and RhoA/RhoA kinase signalling pathways, and decreases the HIF-1 $\alpha$ -induced transcription of Pgp. As a result, Dox accumulates inside MDR+ cells at sufficient amounts to induce cytotoxicity and promote CRT exposure, turning the phenotype of these cells from a chemoimmunoresistant phenotype into a chemoimmunosensitive phenotype.

doi:10.1371/journal.pone.0060975.g007

activity might also be regarded as a potential “Achille’s” heel of MDR+ cells because targeting the Mev pathway with appropriate inhibitors, such as ZA, can interrupt the pathways that sustain both chemo-and immune-resistance (Figure 7B). Overall, these results pave the way to the development of novel chemo-immunotherapy approaches based on the combination of selected chemotherapy drugs with Mev pathway targeting-agents.

## Supporting Information

**Figure S1 Effects of different combinations of ZA and doxorubicin on the intracellular doxorubicin accumulation.** HT29, HT29-dx and HMM cells were treated with 1  $\mu\text{mol/L}$  Dox alone or Dox in combination with 1  $\mu\text{mol/L}$  ZA under different conditions: 1) Dox and ZA were co-incubated for 48 h (ZA & Dox); 2) Dox was added first for 24 h, ZA was added for a further 48 h (Dox+ZA); 3) ZA was added first for 48 h, Dox was added for a further 24 h (ZA+Dox). Intracellular Dox concentrations were significantly higher in HT29 than in HT29-dx and HMM cells (\* $p < 0.001$ ). In MDR+ cells, intracellular Dox concentrations were significantly higher than untreated cells only when ZA preceded Dox (HT29-dx:  $\circ p < 0.05$ ; HMM:  $\diamond p < 0.02$ ). Bars represent the mean  $\pm$  SD of 3 independent experiments. (TIF)

**Figure S2 Biotinylation assays to detect surface calreticulin.** HT29, HT29-dx, and HMM cells after incubation with ZA and/or Dox. Tumor cells were incubated for 48 h without (CTRL) or with 1  $\mu\text{mol/L}$  ZA, for 24 h with 1  $\mu\text{mol/L}$  Dox, for 48 h with 1  $\mu\text{mol/L}$  ZA, followed by 1  $\mu\text{mol/L}$  Dox for a further 24 h (ZA+Dox). Surface CRT was measured in biotinylated extracts; total CRT was measured in the whole cell lysates from the same cells by Western blotting. The results are representative data from one of 2 experiments. (TIF)

## References

- Swanson KM, Hohl RJ (2006) Anti-Cancer Therapy: Targeting the Mevalonate Pathway. *Curr Cancer Drug Targets* 6: 15–37.
- Clendening JW, Pandya A, Boutrosa PC, El Ghamrasni S, Khosravi F, et al. (2010) Dysregulation of the mevalonate pathway promotes transformation. *Proc Natl Acad Sci* 107: 15051–15056.
- Freed-Pastor WA, Mizuno H, Zhao X, Langerod A, Moon S-H, et al. (2012) Mutant p53 disrupts mammary tissue architecture via the mevalonate pathway. *Cell* 148: 244–258.
- Gottesman MM, Fojo T, Bates SE (2002) Multidrug resistance in cancer: role of ATP-dependent transporters. *Nat Rev Cancer* 2: 48–58.
- Troost J, Lindenmaier J, Haefeli WE, Weiss J (2004) Modulation of cellular cholesterol alters P-glycoprotein activity in multidrug-resistant cells. *Mol Pharmacol* 66: 1332–1339.
- Schmidmaier R, Baumann P, Simsek M, Dayyani F, Emmerich B, et al. (2004) The HMG-CoA reductase inhibitor simvastatin overcomes cell adhesion mediated drug resistance (CAM-DR) in multiple myeloma by geranylgeranylation of Rho protein and activation of Rho kinase. *Blood* 104: 1825–1832.
- Riganti C, Orecchia S, Pescarmona GP, Betta PG, Ghigo D, et al. (2006) Bosia A. Statins revert doxorubicin resistance via nitric oxide in malignant mesothelioma. *Int J Cancer* 119: 17–27.
- Mattarollo SR, Loi S, Duret H, Ma Y, Zitvogel L, et al. (2011) Pivotal Role of Innate and Adaptive Immunity in Anthracycline Chemotherapy of Established Tumors. *Cancer Res* 71: 4809–4820.
- Obeid M, Tesniere A, Ghiringhelli F, Fimia GM, Apetoh L, et al. (2007) Calreticulin exposure dictates the immunogenicity of cancer cell death. *Nat Med* 13: 54–61.
- Apetoh L, Mignot G, Panaretakis T, Kroemer G, Zitvogel L (2008) Immunogenicity of anthracyclines: moving towards more personalized medicine. *Trends Mol Med* 14: 141–151.
- De Boo S, Kopecka J, Brusa D, Gazzano E, Matera L, et al. (2009) iNOS activity is necessary for the cytotoxic and immunogenic effects of doxorubicin in human colon cancer cells. *Mol Cancer* 8:e108.
- Clézardin P, Massaia M (2010) Nitrogen-containing bisphosphonates and cancer immunotherapy. *Curr Pharm Des* 16: 3007–3014.

**Figure S3 CD86 expression on DC surface after internalization of MDR+ HT29-dx tumor cells.** The CD86 expression was evaluated on DC surface in the immature status and after internalization of ZA and/or Dox-treated HT29-dx cells. The internalization of ZA+Dox treated-HT29dx cells induced an up-regulation of CD86 expression, in line with the concept that the exposure of DCs to Dox-treated tumor cells stimulates their maturation. The results represent the mean  $\pm$  SD of 6 independent experiments. (TIF)

**Figure S4 Cytotoxic activity of T cells against MDR+ HT29-dx tumor cells.** The cytotoxic activity exerted by T cells against MDR+ HT29-dx tumor cells was evaluated after incubation with autologous DCs pulsed with medium alone (CTRL), ZA, Dox and ZA+Dox-treated HT29-dx cells. Cytotoxicity was evaluated by CFSE staining of tumor target cells identifying the CFSE-labeled dead cells by propidium iodide. The highest cytotoxic activity was observed after T-cell stimulation by DCs loaded with HT29-dx cells exposed to ZA plus Dox. The results are from one experiment. (TIF)

## Acknowledgments

We are grateful to Mr. Costanzo Costamagna for technical assistance and to Mr. Andrew Martin Garvey for editorial assistance.

## Author Contributions

Conceived and designed the experiments: CR AB MM. Performed the experiments: CR BC JK IC. Analyzed the data: CR MC GP MM. Contributed reagents/materials/analysis tools: MC. Wrote the paper: CR BC DG AB MM.

- Coscia M, Quaglino E, Iezzi M, Curcio C, Pantaleoni F, et al. (2010) Zoledronic acid repolarizes tumor-associated macrophages and inhibits mammary carcinogenesis by targeting the mevalonate pathway. *J Cell Mol Med* 14: 2803–2815.
- Fiore F, Castella B, Nuschak B, Bertieri R, Mariani S, et al. (2007) Enhanced ability of dendritic cells to stimulate innate and adaptive immunity on short-term incubation with zoledronic acid. *Blood* 10: 921–927.
- Castella B, Riganti C, Fiore F, Pantaleoni F, Caneparo ME, et al. (2011) Immune modulation by zoledronic acid in human myeloma: an advantageous cross-talk between V $\gamma$ 9V $\delta$ 2 T cells,  $\alpha\beta$  CD8+ T cells, regulatory T (Treg) cells, and dendritic cells. *J Immunol* 187: 1578–1590.
- Castella B, Vitale C, Coscia M, Massaia M (2011) V $\gamma$ 9V $\delta$ 2 T cell-based immunotherapy in hematological malignancies: from bench to bedside. *Cell Mol Life Sci* 68: 2419–2432.
- Morgan C, Lewis PD, Jones RM, Bertelli G, Thomas GA, et al. (2007) The in vitro anti-tumor activity of zoledronic acid and docetaxel at clinically achievable concentrations in prostate cancer. *Acta Oncol* 46: 669–677.
- Ottewell PD, Lefley DV, Cross SS, Evans CA, Coleman RE, et al. (2009) Sustained inhibition of tumor growth and prolonged survival following sequential administration of doxorubicin and zoledronic acid in a breast cancer model. *Int J Cancer* 126: 522–532.
- Coleman RE, Winter MC, Cameron D, Bell R, Dodwell D, et al. (2010) The effects of adding zoledronic acid to neoadjuvant chemotherapy on tumor response: exploratory evidence for direct anti-tumor activity in breast cancer. *Br J Cancer* 102: 1099–1105.
- Riganti C, Miraglia E, Viariso D, Costamagna C, Pescarmona G, et al. (2005) Nitric Oxide reverts the resistance to doxorubicin in human colon cancer cells by inhibiting the drug efflux. *Cancer Res* 65: 516–525.
- Kopecka J, Campia I, Olivero P, Pescarmona G, Ghigo D, et al. (2011) A LDL-masked liposomal-doxorubicin reverses drug resistance in human cancer cells. *J Contr Rel* 149: 196–205.
- Riganti C, Pinto H, Bolli E, Belisario DC, Calogero RA, et al. (2011) Atorvastatin modulates anti-proliferative and pro-proliferative signals in Her2/neu-positive mammary cancer. *Biochem Pharmacol* 82: 1079–1089.
- Laufs U, Liao JK (2000) Targeting Rho in cardiovascular disease. *Circ Res* 87: 526–528.

24. Doublier S, Belisario DC, Polimeni M, Annaratone L, Riganti C, et al. (2012) HIF-1 activation induces doxorubicin resistance in MCF7 3-D spheroids via P-glycoprotein expression: a potential model of the chemo-resistance of invasive micropapillary carcinoma of the breast. *BMC Cancer* 12:e4.
25. Kopecka J, Campia I, Brusa D, Doublier S, Matera L, et al. (2011) Nitric oxide and P-glycoprotein modulate the phagocytosis of colon cancer cells. *J Cell Mol Med* 15: 1492–1504.
26. Betts MR, Brenchley JM, Price DA, De Rosa SC, Douek DC, et al. (2003) Sensitive and viable identification of antigen-specific CD8+ T cells by a flow cytometric assay for degranulation. *J Immunol Meth* 281: 65–78.
27. Stresing V, Daubiné F, Benzaid I, Monkkonen H, Clézardin P (2007) Bisphosphonates in cancer therapy. *Cancer Lett* 257: 16–35.
28. Daubiné F, Le Gall C, Gasser J, Green J, Clézardin P (2007) Antitumor effects of clinical dosing regimens of bisphosphonates in experimental breast cancer bone metastasis. *J Natl Cancer Inst* 99: 322–330.
29. O'Donnell JL, Joyce MR, Shannon AM, Harney J, Geraghty J, et al. (2006) Oncological implications of hypoxia inducible factor-1a (HIF-1a) expression. *Cancer Treat Rev* 32: 407–416.
30. Takata K, Morishige K, Takahashi T, Hashimoto K, Tsutsumi S, et al. (2008) Fasudil-induced hypoxia-inducible factor-1alpha degradation disrupts a hypoxia-driven vascular endothelial growth factor autocrine mechanism in endothelial cells. *Mol Cancer Ther* 7: 1551–1561.
31. Sharma V, Dixit D, Koul N, Mehta VS, Sen E (2011) Ras regulates interleukin-1 $\beta$ -induced HIF-1 $\alpha$  transcriptional activity in glioblastoma. *J Mol Med* 89: 123–136.
32. Zappasodi R, Pupa SM, Ghedini GC, Bongarzone I, Magni M, et al. (2010) Improved clinical outcome in indolent B-cell lymphoma patients vaccinated with autologous tumor cells experiencing immunogenic death. *Cancer Res* 70: 9062–9072.
33. Pallottini V, Guantario B, Martini C, Totta P, Filippi I, et al. (2008) Regulation of HMG-CoA Reductase Expression by Hypoxia. *J Cell Biochem* 104: 701–709.
34. Rohwer N, Cramer T (2011) Hypoxia-mediated drug resistance: novel insights on the functional interaction of HIFs and cell death pathways. *Drug Resist Updat* 14: 191–201.34
35. Eckford PDW, Sharom FJ (2008) Interaction of the P-Glycoprotein Multidrug Efflux Pump with Cholesterol: Effects on ATPase Activity, Drug Binding and Transport. *Biochemistry* 47: 13686–13698.
36. Siczkowski E, Lehner C, Ambros PF, Hohenegger M (2010) Double impact on p-glycoprotein by statins enhances doxorubicin cytotoxicity in human neuroblastoma cells. *Int J Cancer* 126: 2025–2035.
37. Connelly-Smith L, Pattinson J, Grundy M, Shang S, Seedhouse C, et al. (2007) P-glycoprotein is downregulated in KG1a-primitive leukemia cells by LDL cholesterol deprivation and by HMG-CoA reductase inhibitors. *Exp Hematol* 35: 1793–1800.
38. Matsumoto S, Kimura S, Segawa H, Kuroda J, Yuasa T, et al. (2005) Efficacy of the third-generation bisphosphonate, zoledronic acid alone and combined with anti-cancer agents against small cell lung cancer cell lines. *Lung Cancer* 47: 31–39.
39. Pluchino KM, Hall MD, Goldsborough AS, Callaghan R, Gottesman MM (2012) Collateral sensitivity as a strategy against cancer multidrug resistance. *Drug Resist Updat* 15: 98–105.
40. Shukla A, Hillegass JM, MacPherson MB, Beuschel SL, Vacek PM, et al. (2010) Blocking of ERK1 and ERK2 sensitizes human mesothelioma cells to doxorubicin. *Mol Cancer* 9: e314.
41. Ottewell PD, Mönkkönen H, Jones M, Lefley DV, Coleman RE, et al. (2008) Antitumor Effects of Doxorubicin Followed by Zoledronic Acid in a Mouse Model of Breast Cancer. *J Natl Cancer Inst* 100: 1167–1178.
42. Zitvogel L, Kepp O, Kroemer G (2011) Immune parameters affecting the efficacy of chemotherapeutic regimens. *Nat Rev Clin Oncol* 8: 151–160.
43. Kooij G, Backer R, Koning JJ, Reijerkerk A, van Horsen J, et al. (2009) P-Glycoprotein acts as an immunomodulator during neuroinflammation. *PLoSOne* 4: e8212.
44. Takara K, Sakaeda T, Okumura K (2006) An update on overcoming MDR1-mediated multidrug resistance in cancer chemotherapy. *Curr Pharm Des* 12: 273–286.
45. Türk D, Hall MD, Chu BF, Ludwig JA, Fales HM, et al. (2009) Identification of compounds selectively killing multidrug-resistant cancer cells. *Cancer Res* 69: 8293–8301.